DOI:10.1021/cm1011108

CHEMISTRY OF MATERIALS
Article

Low Temperature Atomic Layer Deposition of Tin Oxide

Jaeyeong Heo, Adam S. Hock, and Roy G. Gordon*

Department of Chemistry and Chemical Biology, Harvard University, Cambridge, Massachusetts 02138

Received April 20, 2010. Revised Manuscript Received July 22, 2010

Atomic layer deposition (ALD) of tin oxide (SnO_x) films was achieved using a newly synthesized tin precursor and hydrogen peroxide. We obtained highly pure, conductive SnO_x films at temperatures as low as 50 °C, which was possible because of high chemical reactivity between the new Sn precursor and hydrogen peroxide. The growth per cycle is around 0.18 nm/cycle in the ALD window up to 150 °C, and decreased at higher temperatures. Self-limited growth was demonstrated for both the Sn and O precursors. Thickness is linear in the number of cycles, with an induction period of not more than a few cycles. Rutherford backscattering spectroscopy (RBS) and X-ray photoelectron spectroscopy (XPS) measurements showed that the composition ratio of O/Sn is ~2 and that the films do not contain any detectable carbon or nitrogen impurities. X-ray and electron diffraction analyses identified crystallites of SnO_2 with the rutile structure and average grain size 5−10 nm. The density of the films is 83% of the bulk rutile phase. The surfaces are very smooth, with roughness about 3% of the film thickness. The lowest resistivity is about 10^{-2} ohm·cm. The mobility is over 7 $cm^2/V \cdot s$, and the free electron concentration reaches nearly 10^{20} cm^{-3}. The dependence of mobility on temperature suggests that grain boundary scattering is the dominant electron scattering mechanism. The optical transmission of a 100 nm film is 87.8% and its absorption is 3.3% when averaged over the wavelengths from 400 to 800 nm. Over 80% uniformity of thickness was achieved inside holes with aspect ratios up to 50:1. This successful low temperature growth of conductive nanocrystalline SnO_x films by ALD allows it to be exploited in transparent electrodes for displays, organic light emitting diodes, solar cells, conductive and protective coatings on plastic, microchannel electron multiplier plates, or as a semiconductor layer in transparent transistors.

I. Introduction

Tin oxide has attracted great attention and many uses in recent decades because of its high transparency and conductivity combined with superior stability. It is a semiconductor with band gap (E_g) of ~3.62 eV.[1−3] It shows n-type conductivity due to oxygen vacancies, fluoride or hydroxyl ions replacing oxygen, or metallic dopants such as antimony substituting for tin. Fluorine-doped tin oxide is widely used to reflect infrared heat in energy-conserving low-E windows for buildings.[4] It also serves as a transparent conductor in thin-film solar cells.[5,6] Its dramatic change in conductivity due to charge exchange with absorbed gas species has extended its application to gas sensors for the detection of carbon monoxide or hydrogen.[7−9] Aluminum-doped tin oxide has been reported to be a useful active channel material in thin film transistors, organic light emitting diodes, and flexible displays.[10] One-dimensional nanowires or nanorods of SnO_2, grown by vapor−liquid−solid or by aqueous techniques, show strong ultraviolet photoluminescence.[11,12] Meanwhile, there are several ways to fabricate SnO_x thin films, such as sol−gel method,[13] spray pyrolysis,[14] electron-beam plasma-deposition,[15] sputtering,[10,16] chemical vapor deposition (CVD),[17,18] laser-induced CVD,[19,20] and atomic

*To whom correspondence should be addressed. E-mail: gordon@chemistry.harvard.edu.

(1) Gordon, R. G. *MRS Bull.* **2000**, *25*, 52–57.
(2) Minami, T. *Semicond. Sci. Technol.* **2005**, *20*, S35–S44.
(3) Hartnagel, H. L.; Dawar, A. L.; Jain, A. K.; Jagadish, C. *Semiconducting Transparent Thin Films*; IOP: Bristol, U.K., 1995.
(4) Gordon, R. G. *J. Non-Cryst. Solids* **1997**, *218*, 81–91.
(5) Proscia, J.; Gordon, R. G. *Thin Solid Films* **1992**, *214*, 175–187.
(6) Gordon, R. G.; Proscia, J.; Ellis, F. B., Jr.; Delahoy, A. E. *Sol. Energy Mater.* **1989**, *18*, 263–281.
(7) Rosental, A.; Tarre, A.; Gerst, A.; Sundqvist, J.; Hårsta, A.; Aidla, A.; Aarik, J.; Sammelselg, V.; Uustare, T. *Sens. Actuators, B* **2003**, *93*, 552–555.
(8) Du, X.; Du, Y.; George, S. M. *J. Phys. Chem. A* **2008**, *112*, 9211–9219.
(9) Du, X.; George, S. M. *Sens. Actuators, B* **2008**, *135*, 152–160.
(10) Huh, M. S.; Yang, B. S.; Lee, J.; Heo, J.; Han, S. J.; Yoon, K.; Yang, S.-H.; Hwang, C. S.; Kim, H. J. *Thin Solid Films* **2009**, *518*, 1170–1173.
(11) Chen, R.; Xing, G. Z.; Gao, J.; Zhang, Z.; Wu, T.; Sun, H. D. *Appl. Phys. Lett.* **2009**, *95*, 061908.
(12) Vayssieres, L.; Graetzel, M. *Angew. Chem., Int. Ed.* **2004**, *43*, 3666–3670.
(13) Maddalena, A.; Maschio, R. D.; Diré, S.; Raccanelli, A. *J. Non-Cryst. Solids* **1990**, *121*, 365–369.
(14) Bruneaux, J.; Cachet, H.; Froment, M.; Messad, A. *Thin Solid Films* **1991**, *197*, 129–142.
(15) Isono, T.; Fukuda, T.; Nakagawa, K.; Usui, R.; Satoh, R.; Morinaga, E.; Mihara, Y. *J. SID* **2007**, *15*, 161–166.
(16) Howson, R. P.; Barankova, H.; Spencer, A. G. *Thin Solid Films* **1991**, *196*, 315–321.
(17) Tarey, R. D.; Raju, T. A. *Thin Solid Films* **1985**, *128*, 181–189.
(18) Sundqvist, J.; Lu, J.; Ottosson, M.; Hårsta, A. *Thin Solid Films* **2006**, *514*, 63–68.
(19) Szuber, J.; Czempik, G.; Larciprete, R.; Adamowicz, B. *Sens. Actuators, B* **2000**, *70*, 177–181.
(20) Szuber, J.; Czempik, G.; Larciprete, R.; Koziej, D.; Adamowicz, B. *Thin Solid Films* **2001**, *391*, 198–203.

Published on Web 08/11/2010
© 2010 American Chemical Society

layer deposition (ALD).[9,18,21−27] Among them, ALD is one of the most promising, allowing one to obtain highly conformal materials, thanks to layer-by-layer build-up of material.[28−33] ALD has been known for its excellent thickness and composition controllability as well as pin-hole free films of high density.

The demand for establishing low temperature ALD processes is high especially for the area of thermally sensitive materials such as organic light emitting diodes and photovoltaic cells.[34] One important requirement for achieving low temperature ALD is to find a precursor with appropriate reactivity that leads to clean reactions with the counterpart reactant gas at low growth temperature.[30] Virolla et al. reported ALD-growth of SnO_x using $SnCl_4$ and water at 500 °C.[21] The deposited film was crystalline, but the growth temperature of 500 °C is so high that it cannot be exploited in organic light emitting diodes or flexible display applications. Drozd et al. used alkyltin compounds such as Me_4Sn and Et_4Sn with NO_2 as oxidant gas to form SnO_x thin films in the temperature range of 250−450 °C, which is still a relatively high temperature range.[25] Tarre et al. compared the film quality of SnO_x using two different precursor combinations, $SnCl_4/H_2O_2$ (hydrogen peroxide) and SnI_4/O_2.[27] The maximum growth rate was obtained from 250 to 400 °C and 500−750 °C for each reaction, respectively. Du et al. studied the reaction mechanism of $SnCl_4$ and H_2O_2 and explored the possible application of SnO_x films as CO gas sensors.[8,9,26] Still, these ALD reactions have potential disadvantages of using halogenated Sn precursors such as corrosive damage to growing films and deposition equipment as well as high growth temperatures. Elam et al. reported the possibility of low temperature ALD process for SnO_x film using a non-halogenated Sn precursor, tetrakis(dimethylamino)tin, and H_2O_2 as an oxidant gas at deposition temperatures of 50−300 °C.[22] However, high temperature annealing was required to oxidize and crystallize the amorphous films that have relatively low density and refractive index for growth temperatures below 200 °C. Choi et al. reported plasma-enhanced ALD-SnO_x using dibutyl tin diacetate and O_2 plasma at 200−400 °C.[24] This process requires a complex plasma reactor that produces non-uniform films inside narrow structures with high aspect ratios.

Until now, there has been no report of crystalline SnO_x films grown by thermal ALD at temperature below 200 °C. Meanwhile, Li et al. reported a new scheme for synthesizing a monomeric saturated N-heterocyclic silylene.[35] Following a synthesis scheme similar to the one that they reported, we were able to synthesize a new Sn precursor and explored its potential as a precursor for SnO_2 film formation by ALD. There have been several studies in ALD that used H_2O_2 as an oxidant gas because of its high reactivity,[8,9,22,26,27,36,37] and we found out that our new Sn precursor also has a high reactivity with H_2O_2. With the newly synthesized Sn precursor and 50 wt % H_2O_2 as an oxygen source, we successfully obtained conductive and polycrystalline SnO_x films at growth temperatures over 50 °C. Films grown at 120 °C showed resistivity as low as 1.33×10^{-2} ohm·cm without thermal annealing, and the growth rate was as high as 0.18 nm/cycle. We were able to adjust the electrical properties of SnO_x films by varying the number of H_2O_2 injections without losing the high growth rate. Evaluation of the microstructure indicated that as-grown films are composed of nanocrystalline SnO_2 grains 5−10 nm in size. The composition of the SnO_x films varied from $x = 1.6$ to 2.2 depending on the number of H_2O_2 injections. The SnO_x films were also free of impurities. The films are transparent to visible light, with transmission 87.8% averaged over wavelengths from 400 to 800 nm and 3.3% absorption, for a film 100 nm thick. Over 80% uniformity of thickness was achieved inside narrow holes with a high aspect ratio of ~50:1 (diameter ~200 nm) at 50 °C.

This new process allows low temperature growth of conductive and conformal nanocrystalline SnO_x films. They can be used as transparent electrodes of organic light emitting diodes, polymer solar cells, or other devices for which film formation at low temperature is crucial.

II. Experimental Procedure

Figure 1 shows the molecular structure of the newly synthesized Sn^{2+} precursor: N^2,N^3-di-*tert*-butyl-butane-2,3-diamido-tin(II). The atomic composition of this Sn precursor is $C_{12}H_{26}N_2Sn$. This stannylene complex is readily synthesized from the lithiated diamine[35] (prepared from *N*,*N*′-di-*tert*-butylethylene-diimine and 2 equiv of methyl lithium) and $SnCl_2$ in diethyl ether. The product is isolated by filtration of the reaction mixture to remove LiCl, followed by removal of the solvent and subsequent vacuum sublimation at 60 °C into a cold trap. The Sn precursor obtained from this reaction is solid with a yellowish color. More details of the chemical and physical properties of this Sn precursor will be presented elsewhere.[38] 50 wt % hydrogen peroxide (Sigma Aldrich) was used as received.

(21) Viirola, H.; Niinistö, L. *Thin Solid Films* **1994**, *251*, 127–135.
(22) Elam, J. W.; Baker, D. A.; Hryn, A. J.; Martinson, A. B. F.; Pellin, M. J.; Hupp, J. T. *J. Vac. Sci. Technol. A* **2008**, *26*, 244–252.
(23) Utriainen, M.; Kovacs, K.; Campbell, J. M.; Niinisto, L.; Reti, F. *J. Electrochem. Soc.* **1999**, *146*, 189–193.
(24) Choi, G.; Satyanarayana, L.; Park, J. *Appl. Surf. Sci.* **2006**, *252*, 7878–7883.
(25) Drozd, V. E.; Aleskovski, V. B. *Appl. Surf. Sci.* **1994**, *82/83*, 591–594.
(26) Du, X.; Du, Y.; George, S. M. *J. Vac. Sci. Technol. A* **2005**, *23*, 581–588.
(27) Tarre, A.; Rosental, A.; Aidla, A.; Aarik, J.; Sundqvist, J.; Hårsta, A. *Vacuum* **2002**, *67*, 571–575.
(28) Suntola, T. *Thin Solid Films* **1992**, *216*, 84–89.
(29) Leskelä, M.; Ritala, M. *Thin Solid Films* **2002**, *409*, 138–146.
(30) Leskelä, M.; Ritala, M. *Angew. Chem., Int. Ed.* **2003**, *42*, 5548–5554.
(31) Puurunen, R. L. *J. Appl. Phys.* **2005**, *97*, 121301.
(32) Gordon, R. G.; Hausmann, D.; Kim, E.; Shepard, J. *Chem. Vap. Deposition* **2003**, *9*, 73–78.
(33) George, S. M.; Ott, A. W.; Klaus, J. W. *J. Phys. Chem.* **1996**, *100*, 13121–13131.
(34) Meyer, J.; Schneidenbach, D.; Winkler, T.; Hamwi, S.; Weimann, T.; Hinze, P.; Ammermann, S.; Johannes, H. H.; Riedl, T.; Kowalsky, W. *Appl. Phys. Lett.* **2009**, *94*, 233305.
(35) Li, W.; Hill, N. J.; Tomasik, A. C.; Bikzhanova, G.; West, R. *Organometallics* **2006**, *25*, 3802–3805.
(36) Liang, X.; Lynn, A. D.; King, D. M.; Bryant, S. J.; Weimer, A. W. *ACS Appl. Mater. Interfaces* **2009**, *1*, 1988–1995.
(37) Burton, B. B.; Kang, S. W.; Rhee, S. W.; George, S. M. *J. Phys. Chem. C* **2009**, *113*, 8249–8257.
(38) Hock, A. S.; Gordon, R. G. manuscript in preparation.

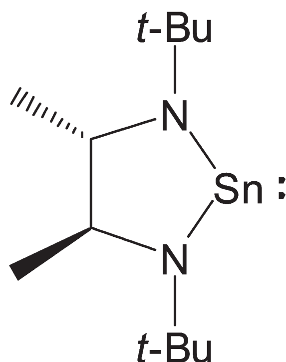

Figure 1. Molecular structure of Sn precursor: N^2,N^3-di-*tert*-butyl-butane-2,3-diamido-tin(II) ($C_{12}H_{26}N_2Sn$).

SnO_x thin films were formed using a custom-built hot-wall ALD reactor. All injection and purge steps were computer-controlled by air-operated valves. The Sn precursor, which was placed in a pyrex container (Kurt J. Lesker) with a vapor volume of 125 mL, was heated to 40 °C, at which temperature it has a vapor pressure of 0.42 Torr. High-purity nitrogen was injected into this vapor volume up to a total pressure of 26 Torr, forming a gas mixture of 1.6% Sn precursor and 98.4% N_2. Before each single injection of Sn precursor or H_2O_2, the reactor pressure was decreased to ~50 mTorr by stopping nitrogen flow into the reactor while evacuating the reactor. Next, a valve between the evacuated reactor and the pump was closed. The gas mixture was then allowed to expand from the trapped volume into the previously evacuated reactor, yielding a final pressure of 5.5 Torr in the reactor. During each of these injection steps, the reactor volume remained isolated from the pump for 3 s. After exposure to each of these doses, the valve between the reactor and the pump was opened, and high-purity N_2 flowed through the reactor as a purge gas. The reactor pressure during these purge steps was set to 300 mTorr by a needle valve. H_2O_2 was vaporized into a trap volume (35 mL) made of stainless steel and subsequently delivered to the reactor without any nitrogen assist. Unlike a conventional ALD system, where the exposure is controlled by an injection time, we varied the exposure by changing the number of injections per ALD cycle. About 2.3 micromoles of tin precursor and 2.9 micromoles of H_2O_2 were estimated to be injected into the reactor (volume = 0.627 L) by one exposure from each trap volume. Although these amounts of tin precursor and of H_2O_2 from a single injection were not enough to reach saturated growth, these small trap volumes allowed careful study of the approach to saturation and the film properties as a function of the number of doses. The addition of well-controlled amounts of H_2O_2 turned out to be critical to obtain SnO_x films with low resistivity.

One growth cycle consists of four steps: *x*-times repetition of the pump down step and the exposure of the Sn precursor and purge of the precursor, *y*-times repetition of the pump down step and the exposure of H_2O_2 and purge of the oxidant. Saturated growth was observed when three doses each of Sn precursor and H_2O_2 were used at 120 °C. The purge time for each step was optimized to be 25 and 45 s, respectively, when the deposition temperature was higher than 100 °C. When the deposition temperature was below 100 °C, a longer H_2O_2 purge time of 100 s was employed to prevent CVD from a vapor mixture.

The resistivity of films deposited on 300 nm-thick thermal oxide/Si substrates was evaluated using a four-point probe, and also corroborated by using the van der Pauw method.[39] The measurement of film thickness and refractive index was performed on a spectroscopic ellipsometer (Woollam, WVASE32). On HF-dipped, H-terminated Si substrate, retardation of nucleation equal to about 25 cycles was observed. For enhancing the nucleation process, Si substrates were oxidized by UV-ozone treatment under a mercury discharge lamp in air for 3 min. Substrates of glassy carbon were cleaned with 10% aq. HF (5 s), deionized water (30 s), and isopropanol (10 s) prior to drying and UV-ozone for 3 min. Substrates of glass were cleaned with isopropanol (10 s), deionized water (30 s), dried and subjected to UV-ozone for 3 min. Surface morphology of the deposited SnO_x film was observed by using field-emission scanning electron microscopy (FESEM, Zeiss, Ultra 55) and atomic force microscopy (AFM, Asylum, MFP-3D SA). The crystallinity and crystallographic orientation of SnO_x film on a glass substrate was determined by X-ray diffraction (XRD, Scintag, XDS 2000, Cu K_α). High-resolution transmission electron microscopy (HRTEM, Jeol, JEM-2100) was also employed for evaluation on film microstructure. The majority carrier type, carrier concentration, and mobility in the temperature range of 80−350 K were investigated by Hall measurement (Ecopia, HMS-3000). The film composition and impurity incorporation were checked by X-ray photoelectron spectroscopy (XPS, Surface Science, SSX-100) and Rutherford backscattering spectroscopy (RBS). The film density was evaluated by combining RBS and X-ray reflectivity (XRR). Optical transmission of the film was measured by a UV−vis spectrophotometer (Hitachi, U-4001).

III. Results and Discussions

Figures 2a and b show the changes in the growth rate with different numbers of doses of Sn precursor and H_2O_2, respectively. Here, three injections each of H_2O_2 and Sn precursor were employed for each ALD cycle, and the deposition temperature was 120 °C. It is shown in the figures that three injections each of Sn precursor and oxidant are enough to obtain the saturated growth rate. The experimental results discussed below employed this condition if it is not mentioned. The linear plot of the film thicknesses as a function of the number of the growth cycles is shown in Figure 2c. Here, the thickness values were reduced by 2 nm, which corresponds to the thickness of native oxide on a Si substrate. This figure clearly indicates that the film thickness is directly proportional to the number of ALD cycles, which is behavior characteristic of layer-by-layer growth in ALD. From the slope, the growth rate is 0.175 nm/cycle, which is the highest growth rate reported so far at a growth temperature of 120 °C. From the small value of the intercept near the origin, we see that the nucleation takes place promptly on the substrates, with little, if any, delay.

Figure 3 shows the growth rate as a function of the deposition temperature for three injections each of the Sn precursor and H_2O_2. It is seen from this figure that the stable ALD window for the Sn precursor and H_2O_2 is from ~50−150 °C. At temperatures above 150 °C, the growth rate of SnO_x decreased with increasing deposition temperature. Accelerated decomposition of H_2O_2 at high temperature (reduced exposure to H_2O_2) could be a reason for the observed decrease in the growth rate. A decreasing number of surface hydroxyl groups, which subsequently

(39) van der Pauw, L. J. *Philips Res. Repts.* **1958**, *13*, 1–9.

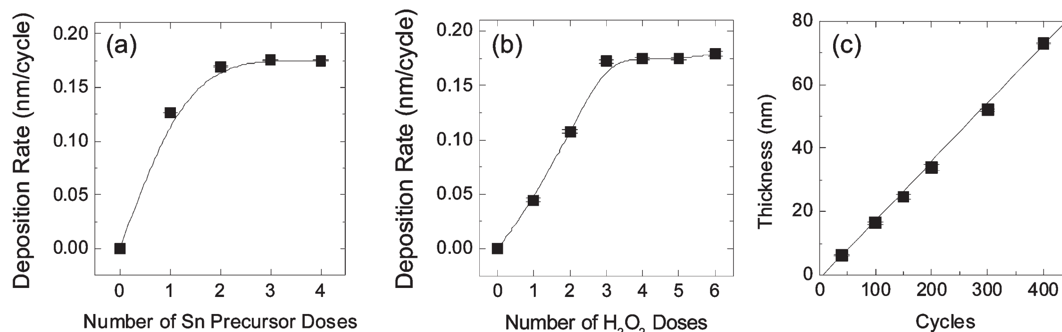

Figure 2. Growth rate for different numbers of injections of (a) Sn precursor and (b) H_2O_2. Three injections of the other precursor were used. The deposition temperature was 120 °C. (c) The thickness of SnO_x films on oxidized Si substrates for three injections of both the Sn precursor and H_2O_2 as a function of the number of growth cycles.

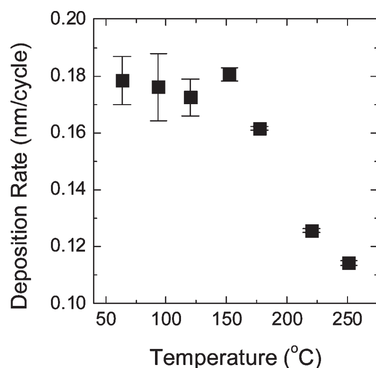

Figure 3. Film growth rate as a function of the deposition temperature. Here, three injections of the Sn precursor and H_2O_2 were used.

act as adsorption sites for Sn precursors, could also limit the amount of growth.[22,29,33,40,41]

When deionized water was used as an oxidant source instead of 50 wt % H_2O_2 while maintaining the other growth conditions, a sharp decrease in the growth rate (to 0.016 nm/cycle) was observed. The difference in the growth rate between 50 wt % H_2O_2 and water as oxidant source was over 10 times. This result indicates that the higher growth rate with the use of 50 wt % H_2O_2 as an oxidant gas comes from the higher reactivity of H_2O_2 with the tin precursor. Also, the large difference in the growth rate corroborates the observed decrease in the growth rate at temperatures above 150 °C, as shown in Figure 2. When hydrogen peroxide thermally decomposes into water and oxygen at high temperatures, neither water nor oxygen strongly reacts with the chemisorbed Sn precursor, unlike H_2O_2.

Figure 4a shows a representative RBS spectrum of an as-deposited SnO_x film using three doses of both the Sn precursor and H_2O_2 on an amorphous carbon substrate heated at 120 °C. All carbon substrates experienced ultraviolet-ozone treatment for 3 min before being loaded into the chamber. Without the treatment, little film was deposited on a carbon substrate because of the paucity of surface functional groups.[42] The O/Sn atomic ratio (calculated[43] from the RBS data) with different numbers of H_2O_2 doses is summarized in Figure 4b. Closed squares and circles represent as-deposited and 350 °C−N_2-annealed states, respectively. As shown in the inset figure of Figure 4a, no nitrogen peak was observed, which clearly indicates that the SnO_x film has no nitrogen impurity. The impurity level of carbon was also negligible from this measurement.

When H_2O_2 was pulsed one time, the O/Sn ratio was 1.62 ± 0.07. The ratio sharply increased with increasing the number of doses from one to two times (1.98 ± 0.02). When the condition of three doses of H_2O_2 was used, the O/Sn ratio was 2.10 ± 0.01. When the oversaturated condition (six doses of H_2O_2) was used, the ratio slightly increased to 2.23 ± 0.05. As shown in Figure 2b, however, the overdose of H_2O_2 does not increase the growth rate, which is the characteristic of ALD,[29−31,33] but it leads to oxygen-rich stoichiometry of SnO_{2+x} as determined by RBS.

Because of the relatively low deposition temperature used, some thermally unstable oxygen species may be incorporated into the films. To check the existence of thermally unstable oxygen species inside the films, annealing was performed at 350 °C for 30 min in a N_2 atmosphere. In Figure 4b, closed circles represent the calculated O/Sn composition ratio for annealed films. The O/Sn ratio decreased slightly after annealing. Notably, the decrease in the ratio was relatively large for the condition of six H_2O_2 doses from 2.23 ± 0.05 to 2.14 ± 0.04, whereas the other conditions show negligible decrease. This result indicates that overdoses of H_2O_2 leave some thermally unstable oxygen species, such as hydroxyl groups, interstitial oxygen, or oxygen at grain boundaries. The existence of a high portion of grain boundaries was verified by high-resolution TEM observations, as discussed later. To further investigate this in situ treatment effect by the excess exposure of H_2O_2 to a film, we performed the following experiment. First, a SnO_x film with three injections of both the Sn precursor and H_2O_2 was deposited at 120 °C for 300 cycles. Post-deposition treatment was done by repeating the same deposition recipe without the Sn injection and the precursor purge steps: the SnO_x film experienced additional 300 exposures to H_2O_2. Although it was performed at the relatively low temperature of 120 °C, the resistivity increased by 15% after the treatment. The

(40) Heo, J.; Won, S.-J.; Eom, D.; Lee, S. Y.; Ahn, Y. B.; Hwang, C. S.; Kim, H. J. *Electrochem. Solid-State Lett.* **2008**, *11*, H210–H213.
(41) Heo, J.; Eom, D.; Lee, S. Y.; Won, S.-J.; Park, S.; Hwang, C. S.; Kim, H. J. *Chem. Mater.* **2009**, *21*, 4006–4011.
(42) Farmer, D. B.; Gordon, R. G. *J. Appl. Phys.* **2007**, *101*, 124503.
(43) Doolittle, L. R. *Nucl. Instrum. Methods Phys. Res. B* **1985**, *9*, 344–351.

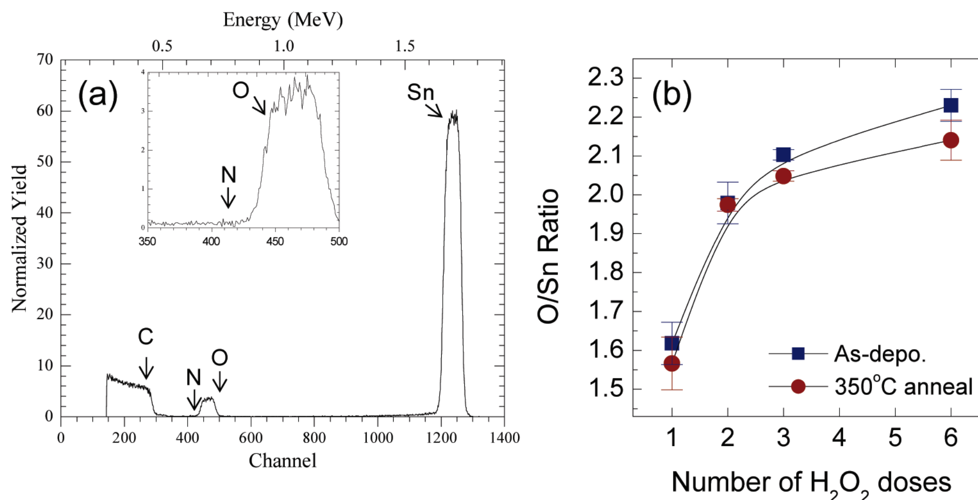

Figure 4. (a) Representative RBS spectrum of SnO_x for three injections of both Sn precursor and H_2O_2. The deposition temperature is 120 °C. The inset figure is an enlarged spectrum with channel ranging from 350 to 500. No nitrogen signal was observed. (b) The simulated O/Sn ratio as a function of the number of H_2O_2 injections. The closed squares and circles represent as-deposited and 350 °C-annealed films, respectively.

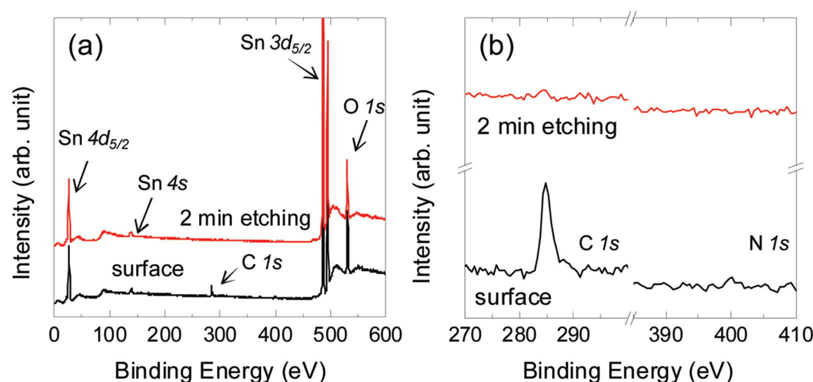

Figure 5. (a) Survey XPS spectra before and after Ar etching for 2 min. (b) XPS spectra for C 1s and N 1s peaks before and after the etching. The SnO_x was deposited using three injections of both the Sn precursor and H_2O_2 at 120 °C.

increase in resistivity after high temperature post-deposition annealing at above 350 °C in oxygen ambient has been reported.[44,45] The change in the O/Sn ratio was also checked by RBS analysis. The O/Sn ratio increased from 2.01 to 2.06 after the additional exposure to H_2O_2. These results clearly indicate that overdose of the strong oxidant affects at least the region near the surface of the film.

Using a metal–organic precursor in vapor deposition always poses a possibility of impurity incorporation especially when the film grows at low temperature. Carbon and nitrogen are typical examples of those impurities. XPS was used to look for impurities in the films. Figure 5a shows the survey scan spectra of as-deposited and 2 min-etched SnO_x films deposited at 120 °C for three doses each of Sn precursor and H_2O_2. In this figure, all peaks except the two peaks at ~285 eV for C 1s and at ~531 eV for O 1s are attributed to Sn. The C 1s peak was observed in the surface spectrum, which may be due to carbon impurities actually incorporated or to surface contamination after air exposure. To find out the origin of the C 1s peak, mild Ar sputtering for 2 min was done. The spectra of the C 1s and N 1s peaks before and after the Ar sputtering are shown in Figure 5b. It is clearly seen in this figure that no C 1s peak was observed after the sputtering. This result indicates that no carbon exists inside the film. In addition, the N 1s (~398 eV) region before and after 2 min Ar etching shows that the deposited SnO_x film has no detectable nitrogen, which might originate from residual precursors that had not been reacted with H_2O_2. Quantitative XPS analysis of an as-deposited SnO_x film surface without any sputtering yielded an O/Sn ratio of 1.76, which is lower than that (2.10) from the RBS measurement, perhaps because of an oxygen deficient surface layer.[46] Even after taking XPS into consideration, the RBS result proves that the bulk composition of films deposited with three doses of H_2O_2 are close to stoichiometric SnO_2.

Figures 6a and b show the high-resolution XPS Sn $3d_{5/2}$ and O 1s spectra after 2 min Ar etching for as-prepared samples with different numbers of H_2O_2 injections, respectively. The deposition temperature was 120 °C and three Sn

(44) Melsheimer, J.; Ziegler, D. *Thin Solid Films* **1983**, *109*, 71–83.
(45) Beensh-Marchwicka, G.; Kròl-Stepniewska, L.; Misiuk, A. *Thin Solid Films* **1984**, *113*, 215–224.
(46) Sanjinés, R.; Coluzza, C.; Rosenfeld, D.; Gozzo, F.; Alméras, P.; Lévy, F.; Margaritondo, G. *J. Appl. Phys.* **1993**, *73*, 3997–4003.

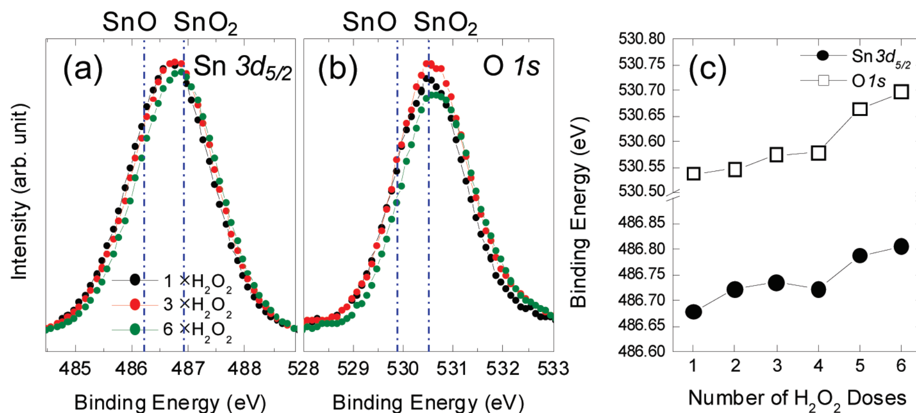

Figure 6. High-resolution XPS (a) Sn $3d_{5/2}$ and (b) O 1s spectra after 2 min Ar etching for the samples with one, three, and six injections of H_2O_2, respectively. (c) The center of each peak is summarized as a function of the number of H_2O_2 injection. The binding energy shift toward higher energy state is clearly seen from the figures with increasing the H_2O_2 injection.

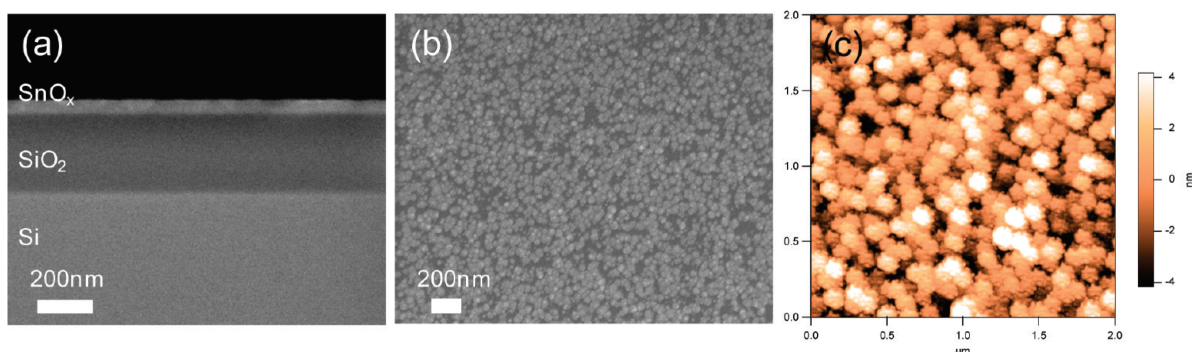

Figure 7. (a) Cross-sectional SEM image of SnO_x film for 400 cycles deposited on a thermal oxide substrate and (b) its plan-view image. Here, the deposition temperature is 120 °C. (c) AFM image of the same film for tapping mode. The root-mean-square roughness is estimated to be ~2 nm.

precursor injections were used. Because of the small differences between all peaks, selected samples (one, three, and six injections) were depicted in both figures. The binding energy of Sn $3d_{5/2}$ peak for stoichiometric SnO and SnO_2 is reported to be 486.2 and 486.9 eV, respectively.[20] The binding energy for the two components in O 1s peak is 529.9 and 530.5 eV with an additional high binding energy peak assigned to chemisorbed and/or hydroxylated oxygen species.[20] Detailed peak deconvolution was skipped because of its complex and arbitrary nature. Instead, the center of the Sn and O peaks was summarized in Figure 6c, which shows the trend of the relative concentrations of SnO and SnO_2 components. As shown in Figures 6a−c, the chemical state of the SnO_x films gets closer to that of stoichiometric SnO_2 with increasing number of H_2O_2 injections. Even the SnO_x film with one injection of H_2O_2 is mostly oxidized, which is reasonable based on the O/Sn ratio of 1.62 determined by RBS analysis. Compared to the case of three injections, a noticeable binding energy shift is observed for the overdose conditions of five and six injections, which is consistent with the increase in the O/Sn ratio (Figure 4b).

Figure 7a shows the cross-sectional SEM image of the SnO_x film deposited at 120 °C with the saturated condition. A 300 nm-thick thermal oxide was used as a substrate, and the growth cycle was repeated 400 times. It is seen from that figure that SnO_x grows smoothly on the thermal oxide. The observed thickness is 69−72 nm, which is consistent with the result (~72 nm) obtained from ellipsometry. Figure 7b shows that the surface morphology of the same film consisted of small and fine grains. Figure 7c shows the surface morphology of the SnO_x film measured by AFM. The small and round-shaped grain structure was also demonstrated by this figure. The root-mean-square (rms) roughness was ~2 nm, which is less than 3% of the film thickness. The surface morphology appears to come from the formation of the crystalline phase in the as-deposited state. The existence of the crystallized grains was confirmed by following X-ray diffraction and TEM analyses. Considering the existence of crystalline phases, its rms roughness value is still low compared to films from other methods,[23] which can be explained by the very small grain size.

The conformal deposition of the SnO_x in a three-dimensional structure was tested on a substrate with various hole sizes and depths with aspect ratio up to 50. When the deposition temperature was set to 120 °C, film thickness was constant up to an aspect ratio of 13:1. Deeper in the holes, the film became thinner. Improvement in the conformality of the SnO_x film was observed after decreasing the deposition temperature, which inevitably accompanies some compromise over the film's conductivity as discussed later (Figure 14d). On the basis of these results, it was concluded that more decomposition of H_2O_2 occurs when the films are deposited at high

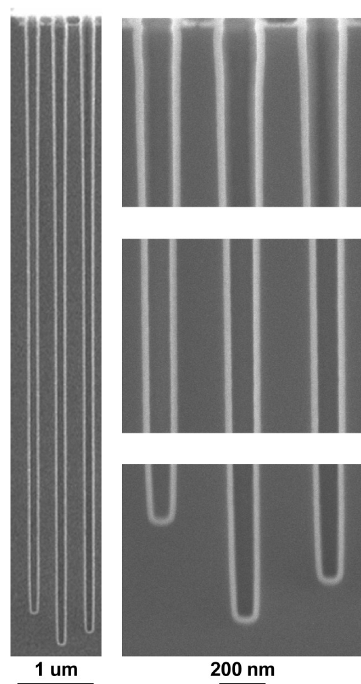

Figure 8. Cross-sectional SEM of holes with aspect ratio 50:1 coated at 50 °C by 190 cycles of ALD SnO_x. Over 80% uniformity of thickness was achieved in narrow holes.

temperature, when H_2O_2 experiences frequent collisions inside narrow holes. A conformal SnO_x film with >80% uniformity was achieved in narrow holes (about 50:1 ratio of depth to diameter, diameter: ~200 nm) at low deposition temperature of 50 °C, as shown in Figure 8. Here, the number of ALD cycles was 190, and three injections of both the Sn precursor and H_2O_2 were used. The three figures on the right-hand panel show high-magnification views of the top, middle, and bottom parts, respectively, of the film inside the hole. When the change in film composition with exposure to H_2O_2 is considered (Figure 4b), the O/Sn ratio may vary with position along the hole because of decreased exposure of H_2O_2 near the bottom, which is difficult to analyze.

Figure 9 shows the X-ray diffraction pattern of a ~100 nm-thick SnO_x film deposited at 120 °C for three injections of the Sn precursor and H_2O_2 on a glass substrate. It is seen from the figure that the SnO_x film exhibits the crystalline structure of rutile SnO_2. The peaks at 34.1°, 38.3°, 51.6°, and 58.3° are assigned to diffraction from the (101), (200), (211), and (002) planes. The intense (110) peak reported at 26.6° was not observed in this figure, but interestingly it was observed in the electron diffraction results discussed below.

Figure 10a shows the plan-view TEM image of ~35 nm-thick SnO_x film (200 cycles) deposited on a 30 nm-thick SiN membrane at 120 °C. The as-deposited SnO_x film on this thin membrane has a polycrystalline structure. A ring-shaped electron diffraction pattern of this film, as shown in Figure 10b, displays the polycrystalline nature of the deposited SnO_x film, which is consistent with the XRD measurement. The diffraction rings are assigned to be (110), (101), (200), (211), and (301) diffractions, respectively.

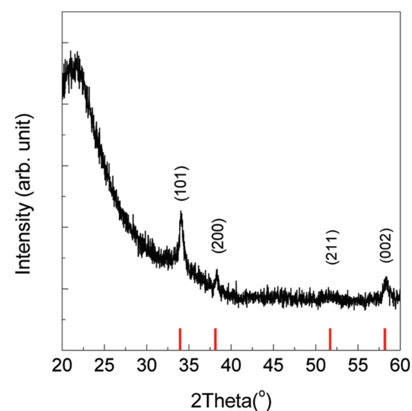

Figure 9. XRD pattern of the ~100 nm-thick SnO_x film grown on a glass substrate at 120 °C. The lines at the bottom of figure are added for each diffraction peak.

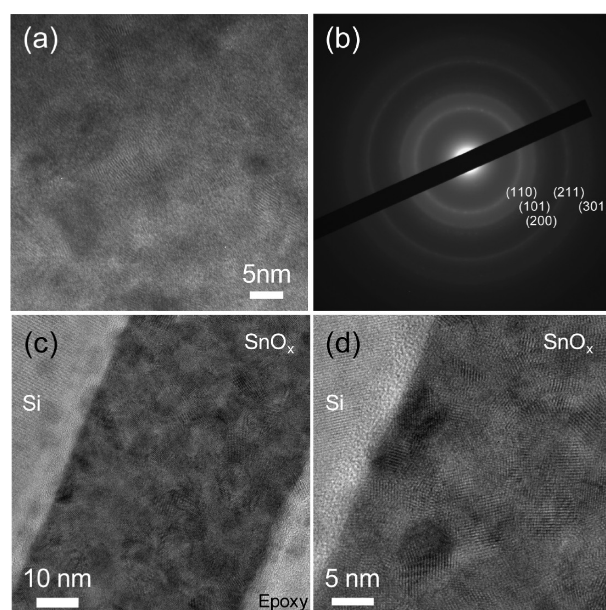

Figure 10. (a) Plan-view TEM image of SnO_x film grown on a 30 nm-thick SiN membrane at 120 °C. (b) Ring-shaped electron diffraction pattern from figure (a). The diffraction rings are assigned to be (110), (101), (200), (211), and (301) plane diffractions. (c) Cross-sectional TEM image of 52 nm-thick SnO_x film on a Si substrate. (d) Cross-sectional high-resolution TEM image of the nanocrystalline SnO_x film. Oxide layer of ~2 nm is observed between a Si substrate and SnO_x film.

The ALD formation of crystalline SnO_2 films at a low temperature of 120 °C has not been reported before. Figure 10c is a representative cross-sectional TEM image of the SnO_x film grown for 300 cycles on a Si substrate. The film thickness of ~52 nm observed by TEM matched with the value from ellipsometry. Nanocrystalline structures in the SnO_x film can be also identified in this figure. Similar structures were found on all substrates that were used. Many grain boundaries are also seen in this figure. From the high resolution image of Figure 10d, the grain size of SnO_x was estimated to be 5−10 nm. About 2 nm-thick native silicon oxide was also observed from this figure.

Figure 11a shows the optical transmission and reflection spectra of the SnO_x film deposited at 120 °C on silica glass and measured by a UV−vis spectrophotometer.

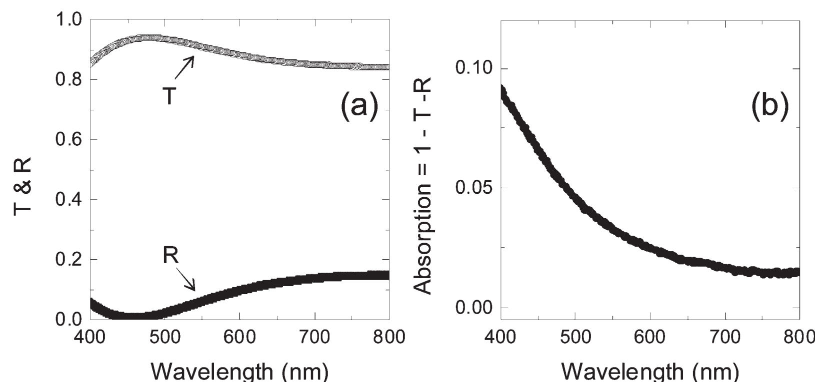

Figure 11. (a) Transmission and reflection spectrum for 100 nm-thick SnO_x film deposited on a silica substrate at 120 °C in the wavelengths from 400 to 800 nm. The average transmission in the region is 87.8%. (b) The calculated absorption in the wavelengths from 400 to 800 nm is 3.3%.

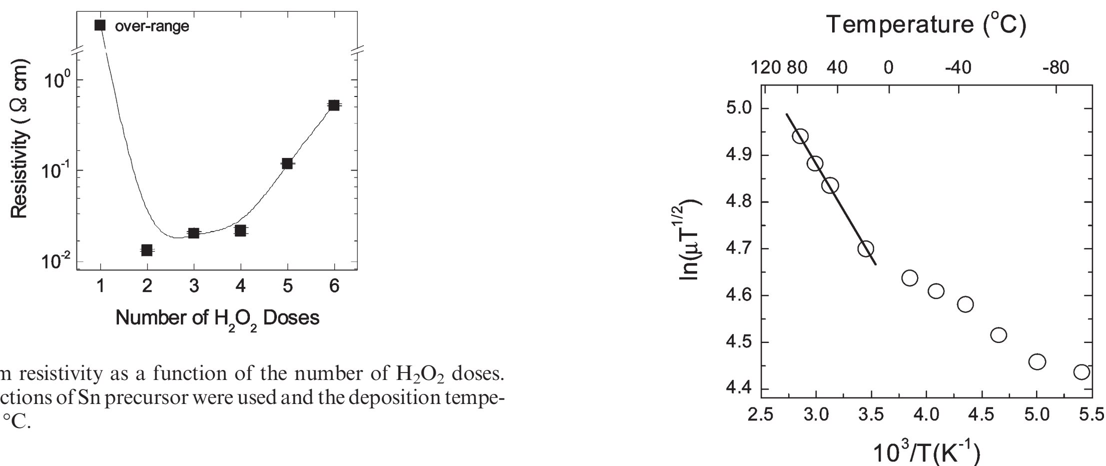

Figure 12. Film resistivity as a function of the number of H_2O_2 doses. Here, three injections of Sn precursor were used and the deposition temperature was 120 °C.

Figure 13. Mobility as a function of temperature as a plot of $\ln(\mu T^{1/2})$ versus $1/T$. Here, the SnO_x was deposited at 120 °C. The straight line for high temperature region indicates that the mobility of electrons in the SnO_x film is mainly limited by grain boundary scattering.

Three injections of both the Sn precursor and H_2O_2 were used, and the film thickness was 100 nm. The background correction was done using an uncoated silica substrate. The average transmission from 400 to 800 nm wavelengths was 87.8%. The average transparency is high enough to be used as a transparent electrode. The absorption spectrum is plotted in Figure 11b. The average absorption was 3.3% from 400 to 800 nm wavelengths.

We found out that the precise control over the exposure of H_2O_2 has a critical impact on the film's electrical properties. Figure 12 plots the film resistivity as a function of the number of H_2O_2 doses in each cycle at 120 °C. The film thicknesses measured by ellipsometry were used to calculate the film resistivity from sheet resistances measured by using four-point probe method. When one dose of H_2O_2 was used, the resistivity of as-deposited film was over 10^5 ohms per square. With the introduction of two H_2O_2 doses, the film shows the lowest resistivity of 1.33×10^{-2} ohm·cm. However, as shown in Figure 2b, the saturated growth rate was not observed for this condition although it is as high as 0.11 nm/cycle. The electrical conductivity of SnO_x can result from oxygen vacancies, which act as majority electron donors.[3,22,23,47,48] When the number of hydrogen peroxide doses is in the range of two to four times, the resistivity remains between 1 and 3×10^{-2} ohm·cm. Although the growth rate was saturated when the number of H_2O_2 doses was higher than three, the film resistivity gradually increased with increasing the number of H_2O_2 doses: 2.2×10^{-2}, 1.2×10^{-1}, and 5.3×10^{-1} ohm·cm for four, five, and six doses of H_2O_2, respectively. The resistivity change as a function of the oxidant exposure is similar to other reports that SnO_x films were formed by electron-beam plasma-deposition,[15] CVD,[49] and ALD,[23] where the resistivity gradually goes up with increasing amounts of the corresponding oxygen sources, after passing its minimum value.

To find the carrier concentration and the mobility of the SnO_x films, Hall measurements were conducted. The carrier concentration of SnO_x film deposited at 120 °C for three injection of both the Sn precursor and H_2O_2 was (−)8.1−9.3 × 10^{19} cm^{-3}. The negative sign confirms that electrons are the majority carriers in the deposited SnO_x films. The mobility of the SnO_x film was 6.4−7.4 $cm^2/V \cdot s$ at room temperature. The electrical properties, that is, carrier concentration, mobility, and resistivity, are comparable to those from the films grown at 400−500 °C using the spray pyrolysis technique[47] or to ones from the conventional magnetron sputtering process.[10] However,

(47) Shanthi, E.; Dutta, V.; Banerjee, A.; Chopra, K. L. *J. Appl. Phys.* **1980**, *51*, 6243–6251.
(48) Batzill, M.; Diebold, U. *Prog. Surf. Sci.* **2005**, *79*, 47–154.
(49) Murty, N. S.; Jawalekar, S. *Thin Solid Films* **1983**, *108*, 277–283.

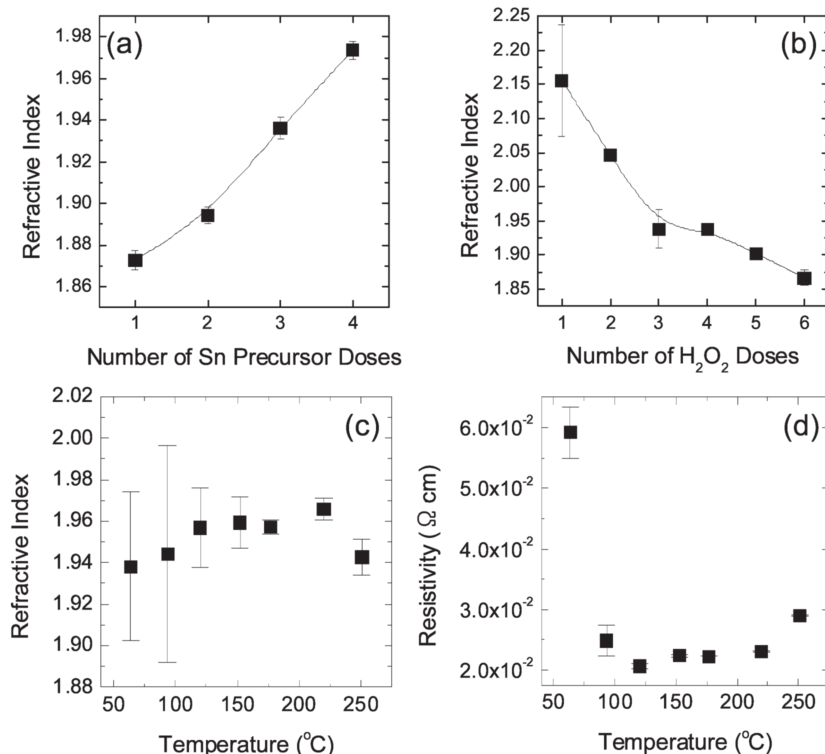

Figure 14. Refractive index with different numbers of injections of the Sn precursor (a) and H_2O_2 (b). Three injections of the other precursor were used. The deposition temperature was 120 °C. The refractive index (c) and resistivity (d) as a function of the deposition temperature.

both the carrier concentration and the mobility for the SnO_x film with six injections of H_2O_2 decreased about 10 times compared to the SnO_x with three injections. It is evident that injection of the oxidant over three times makes over-stoichiometric films, which are electrically more insulating. Excessive exposure of H_2O_2 partially fills oxygen vacancies (decreasing the carrier concentration) and possibly stuffs oxygen species into grain boundaries (decreasing the mobility), which is consistent with the increase in the O/Sn ratio from RBS and XPS analyses. Similarly, Szuber et al. reported increased resistance of an oxygen-rich $SnO_{2.2}$ film deposited by using laser-assisted CVD.[19] For ALD-TiO_x film, excess oxygen composition of 2.2 was reported by Kim et al.,[50] where titanium tetraisopropoxide and ozone were used for Ti precursor and oxidant, respectively. It is possible that these highly oxidizing conditions produce films with excess oxygen to cation ratio like using high concentration of H_2O_2 in this study.

Figure 13 plots the mobility as a function of temperature. Here, a 70 nm-thick SnO_x film deposited at 120 °C with three injections of both the Sn precursor and H_2O_2 was used. The three main scattering mechanisms limiting the observed mobility are optical lattice scattering, ionized impurity scattering, and grain boundary scattering.[3,14] With the carrier concentration higher than 10^{19} cm^{-3}, different scattering mechanisms have been reported. When the carrier concentration of deposited SnO_x film is higher than $\sim10^{19}$ cm^{-3}, Bruneaux et al. reported that the influence of grain boundaries becomes negligible.[14] Shanthi et al.[47] and Islam and Hakim[51] suggested that grain boundary scattering dominates even for high carrier concentrations. The grain boundary scattering dependent mobility is given by eq 1[3,14,47,51]

$$\mu = \mu_0 T^{-1/2} \exp\left(\frac{-\phi_b}{kT}\right) \quad (1)$$

where μ is mobility, μ_0 is pre-exponential term, T is temperature, and ϕ_b is potential barrier height. The plot of $\ln(\mu T^{1/2})$ versus $1/T$ of Figure 13 gives a straight line at higher temperatures (>290 K), which indicates that grain boundary scattering is the dominant mechanism in the as-deposited SnO_x films. There are abundant grain boundaries between the nanocrystalline grains of 5−10 nm size. The extracted grain boundary potential barrier (ϕ_b) was 34 meV, which is comparable to 30 meV from Shanthi et al.'s work[47] and 36−53 meV from Islam and Hakim's work.[51] Below the temperature of 290 K there appears to be a mixed transport region of thermionic emission and tunneling through grain boundaries.[3,52] When degenerate gas behavior was applied, the plot of $\ln(\mu/T)$ versus $1/T$ did not give any increase in μ/T with temperature increase in the range of 200−300 K. Also, no intentional doping of the SnO_x films was performed so that ionized scattering was less important than grain boundary scattering.

Figures 14a and b show the changes in the refractive index with different numbers of Sn precursor and H_2O_2

(50) Kim, S. K.; Lee, S. Y.; Seo, M.; Choi, G.-J.; Hwang, C. S. *J. Appl. Phys.* **2007**, *102*, 024109.

(51) Islam, M. N.; Hakim, M. O. *J. Phys. D: Appl. Phys.* **1986**, *19*, 615–621.

(52) Crowell, C. R.; Rideout, V. L. *Solid-State Electron.* **1969**, *12*, 89–105.

doses, respectively. The deposition temperature was 120 °C. It is seen from these figures that the refractive index is strongly influenced by the number of H_2O_2 doses. Relatively Sn-rich (oxygen deficient) conditions lead to higher refractive index of the films for both cases. The changes in the refractive index correspond to the fact that the refractive indices of SnO and SnO_2 are 2.4 and 2.0, respectively.[22] The refractive index for three injections is about 1.95 and this value is higher than the value of ~1.7 obtained by Elam et al.[22] using the same ALD temperature of 120 °C, and it is similar to CVD films made at higher temperatures of 400−600 °C by Viirola and Niinistö.[21] By RBS and XRR analyses, the film density was estimated to be ~5.61−5.80 g/cm^3 for films grown by using three injections each of the Sn precursor and H_2O_2 at 120 °C. Given the theoretical density of 6.95−6.99 g/cm^3 for bulk SnO_2,[22,48] the film density corresponds to 80−83% of the bulk value. This high film density, which comes from the high reactivity of the precursor with H_2O_2, could be one of the reasons that the SnO_x film shows relatively low resistivity even at low deposition temperatures. In Figure 14b, a gradual decrease in refractive index is observed when the number of H_2O_2 injections is higher than three. As discussed in the RBS (Figure 4) and XPS (Figure 6) results, this trend may be attributed to the excess oxidation effects of H_2O_2. Similarly, Melsheimer et al. reported a decrease in the refractive index of SnO_x films after heat treatment in air with a resistivity increase by a factor of 2−4.[44]

Figure 14c shows that the deposition temperature has little effect on the refractive index. Irrespective of the deposition temperature the refractive indexes of stoichiometric films are ~1.94−1.96, which indicates that the chemical states of the SnO_x films are similar. Figure 14d depicts the change in the film resistivity as a function of the deposition temperature. The film resistivity remains $2-3\times10^{-2}$ ohm·cm except for the one grown at 63 °C. Nitrogen and other impurities were below the detection limit of RBS for the film grown at 63 °C. The extended lifetime of H_2O_2 at lower deposition temperature may oxidize the SnO_x film excessively, which increases the film resistivity. Although the growth rate decreased with increasing the deposition temperature above 150 °C (Figure 3), there was no prominent increase in the film resistivity except for one grown at 250 °C.

On the basis of the experimental results, the low temperature SnO_x process could be used in organic light emitting diodes, organic thin film transistors, or polymer solar cells where the process temperature is a critical factor affecting the performance of the devices. The potential oxidation of those materials because of the usage of H_2O_2 could be an issue since these thermally sensitive materials are generally susceptible to the oxidation as well. We tested the SnO_x process on polymer solar cell materials, but we did not observe any oxidation problem. The usage of measured volumes of vapor in our system allows precise control of the exposure to H_2O_2.

IV. Conclusions

ALD of SnO_x films using a newly synthesized Sn precursor and 50 wt % hydrogen peroxide was investigated. It was possible to achieve high-purity and conductive SnO_x films at a deposition temperature as low as 50 °C because of the high reactivity of hydrogen peroxide with the Sn precursor. The lowest resistivity obtained was 1.33×10^{-2} ohm·cm. RBS and XPS measurements confirmed that the films have no detectable carbon or nitrogen impurities. XRD and TEM analyses showed that the SnO_x film consists of nanocrystalline grains of 5−10 nm size having the usual crystal structure of bulk SnO_2. Over 80% uniformity of thickness was achieved in narrow holes with an aspect ratio of 50:1 at 50 °C. A 100 nm thick film has transmission of 87.8% and absorption of 3.3% averaged over the wavelength from 400 to 800 nm. The change in the mobility with temperature revealed that grain boundary scattering is the dominant electron scattering mechanism. The exposure of H_2O_2 played a key role to determine the film's overall properties, so careful control of the exposure of H_2O_2 is needed for deposition of SnO_x with well-controlled properties. The low temperature growth of conductive nanocrystalline SnO_x film allows its application to thermally sensitive devices such as organic light emitting diodes, organic thin film transistors, solar cells, electron multipliers or conductive and protective coatings on plastics.

Acknowledgment. Support from the Camille and Henry Dreyfus Postdoctoral Program in Environmental Chemistry is gratefully acknowledged. This work was performed in part at the Center for Nanoscale Systems (CNS) at Harvard University, a member of the National Nanotechnology Infrastructure Network (NNIN), which is supported by the National Science Foundation under NSF award no. ECS-0335765. The authors acknowledge the assistance of Yiqun Liu, Zhefeng Li, and Prasert Sinsermsuksakul for analysis of film properties and Dr. Wontae Noh for editing.